Growth and Form of Planetary Seedlings: Results from a Microgravity Aggregation Experiment

J. Blum,[1,*] G. Wurm,[2] S. Kempf,[3] T. Poppe,[1] H. Klahr,[4] T. Kozasa,[5] M. Rott,[6] T. Henning,[1] J. Dorschner,[1] R. Schräpler,[1] H. U. Keller,[7] W. J. Markiewicz,[7] I. Mann,[7] B. A. S. Gustafson,[8] F. Giovane,[9] D. Neuhaus,[10] H. Fechtig,[3] E. Grün,[3] B. Feuerbacher,[10] H. Kochan,[10] L. Ratke,[10] A. El Goresy,[11] G. Morfill,[12] S. J. Weidenschilling,[13] G. Schwehm,[14] K. Metzler,[15] and W.-H. Ip[16]

[1]*Astrophysical Institute and University Observatory, University of Jena, Schillergässchen 2-3, 07745 Jena, Germany*
[2]*Laboratory for Atmospheric and Space Physics, University of Colorado, Campus Box 392, Boulder, Colorado 80309-0392*
[3]*Max-Planck-Institut für Kernphysik, Saupfercheckweg 1, 69117 Heidelberg, Germany*
[4]*UCO/Lick Observatory, Kerr Hall, University of California, Santa Cruz, California 95064*
[5]*Division of Earth and Planetary Sciences, Graduate School of Science, Hokkaido University, Sapporo 060-0810, Japan*
[6]*Fachgebiet Raumfahrttechnik, Technische Universität München, Boltzmannstrasse 15, 85748 Garching, Germany*
[7]*Max-Planck-Institut für Aeronomie, Max-Planck-Straße 2, 37191 Katlenburg-Lindau, Germany*
[8]*Department of Astronomy, 211 Bryant Space Science Center, University of Florida, Gainesville, Florida 32611-2055*
[9]*Space Science Division, Naval Research Laboratory, 4555 Overlook Avenue SW, Washington, D.C. 20375-5320*
[10]*Institut für Raumsimulation, Deutsches Zentrum für Luft- und Raumfahrt DLR, 51140 Köln, Germany*
[11]*Max-Planck-Institut für Chemie, Joh.-Joachim-Becher-Weg 27, 55128 Mainz, Germany*
[12]*Max-Planck-Institut für extraterrestrische Physik, Giessenbachstraße, 85748 Garching, Germany*
[13]*Planetary Science Institute, 620 North Sixth Avenue, Tucson, Arizona 85705-8331*
[14]*ESA/ESTEC, Keplerlaan 1, 2200 AG Noordwijk, The Netherlands*
[15]*Museum für Naturkunde, Institut für Mineralogie, Invalidenstraße 43, 10099 Berlin, Germany*
[16]*Institute of Space Science, National Central University, Chung-Li, Taiwan, Republic of China*
(Received 27 July 2000)

The outcome of the first stage of planetary formation, which is characterized by ballistic agglomeration of preplanetary dust grains due to Brownian motion in the free molecular flow regime of the solar nebula, is still somewhat speculative. We performed a microgravity experiment flown onboard the space shuttle in which we simulated, for the first time, the onset of free preplanetary dust accumulation and revealed the structures and growth rates of the first dust agglomerates in the young solar system. We find that a thermally aggregating swarm of dust particles evolves very rapidly and forms unexpected open-structured agglomerates.

PACS numbers: 96.35.Cp, 45.70.–n, 61.43.Hv, 81.10.Mx

It is now widely accepted that planets form from the nebula of gas and dust that comprises nascent solar systems. Inelastic, adhesive collisions between these dust particles eventually form kilometer-sized bodies, called planetesimals, which then collide under the influence of their mutual gravity to form planets [1–6]. After condensation of the micron-sized dust grains in the cooling gas, these initially collide with each other due to thermal (Brownian) motion, and, by adhesion due to van der Waals forces, form aggregates. The agglomeration rate of freshly condensed [7,8] preplanetary dust grains is determined by three factors: the collision cross section, the collision velocity, and the sticking probability of the dust particles, which are mutually interdependent. Laboratory experiments with micron-sized solid particles and dust agglomerates thereof have shown that, for moderate collision velocities $v_c \leq 1\ \mathrm{m\,s^{-1}}$, the sticking probability is always unity [9–11]. The collision cross section and the collision velocity strongly depend on the morphology of the interacting preplanetary dust aggregates. Open-structured, fluffy particles generally have a larger cross section than compact grains, but couple also much better to the gas motion, so that relative velocities between fluffy agglomerates are suppressed. The gas-grain interaction is best described by the dust particles' response time to the gas motion, τ_f. In the free molecular flow regime, $\tau_f \propto \frac{m}{\sigma_a}$, where m and σ_a are the mass and the geometrical cross section (i.e., the projected area) of the dust aggregate. Aggregation models [1,12] for the Brownian motion-driven dust growth predict a scenario in which dust clusters of similar mass predominantly contribute to the agglomeration process. This leads to the evolution of a quasimonodisperse distribution of aggregate masses and to a relation between aggregate mass and size s of

$$m \propto s^{D_f}, \tag{1}$$

with an exponent ("fractal dimension") in the range of $D_f \approx 1.8$–2.1. For quasimonodisperse systems, the mean aggregate mass grows by a power law in time, $m(t) \propto t^z$, and is related to the mass dependence of the collision cross section $\sigma_c \propto m^\mu$ and the collision velocity $v_c \propto m^\nu$ of the aggregating particles through $\mu + \nu = \frac{z-1}{z}$ (e.g., see the review in [13]). Here, z, μ, and ν are the respective exponents of the assumed power law functions for $m(t)$, $\sigma_c(m)$, and $v_c(m)$. Fractal aggregates with $D_f \approx 2$ have $\mu \approx 1$, and ballistic thermal collisions yield $\nu = -\frac{1}{2}$. Thus, we expect $z \approx 2$, which is supported by numerical simulations [12,13].

 0031-9007/00/85(12)/2426(4)$15.00

Aggregation due to Brownian motion in a cloud of micron-sized particles in rarefied gases has never been investigated experimentally, and there is no empirical evidence indicating how planetary formation begins and evolves. These agglomeration studies require an environment free from the overwhelming effect of sedimentation in Earth's gravitational field. For the first experimental investigation of the initial preplanetary growth stage and for a test of the present models, we designed and built the Cosmic Dust Aggregation Experiment CODAG [14,15], which flew onboard STS-95 in October 1998. A sample of monodisperse, spherical SiO_2 (glass) dust grains (particle radii $s_0 = 0.95\ \mu$m; monomer masses $m_0 = 7.2 \times 10^{-15}$ kg) was dispersed into a rarefied gas of pressure $p = 0.75$ mbar and temperature $T = 300$ K. Because of the low gas pressure, a molecular gas flow around the dust grains was present, and the particle motion close to the contact of two dust grains was ballistic (as opposed to the diffusive overall motion of the dust), so that the experimental conditions matched those in young solar systems very well.

The dust particle motion and the structure of the grown dust aggregates were analyzed with a stereo long-distance microscope with attached high-speed digital CCD cameras. The field of view of each of the two microscopes was 0.25×0.25 mm^2, with a spatial resolution of 1 μm, a depth of field of $\sim$80 μm, and a temporal resolution of 5 ms.

In the experiment, the dust was not perfectly homogeneously distributed throughout the experiment chamber, but the dust particles were preferably found within two cloudlets, which were surrounded by basically dust-free zones. The cloudlets slowly drifted through the experiment chamber with a velocity of 0.4 mm s^{-1} and crossed the field of view of the microscopes approximately $t = 55$ s and $t = 100$ s after the dust injection. Figure 1a shows microscope raw images of typical dust particles (top row) and the result of the image analysis (bottom row) by which we reduced each picture to its substantial information. For the experimental run of interest, we detected twelve well-focused dust aggregates, five of which were simultaneously imaged by both microscopes (see Fig. 1b for two-dimensional and Fig. 1c for three-dimensional representations of one of these aggregates). The two-dimensional images were used to derive the radius of gyration and the geometrical cross section of each of the aggregates. It turned out that the aggregates have an unexpectedly high average ratio of maximum to minimum radius of gyration of $\rho \approx 3.5$, which means that they are highly elongated. Published values for dust aggregates grown in a turbulent gas flow fall in the range $\rho \approx 2$–3 [16]. An analysis of the spatial orientation of the maximum radius of gyration showed that our dust aggregates were randomly oriented, i.e., unaligned. This means that the elongated structures are not the result of a preferential orientation of the dust grains.

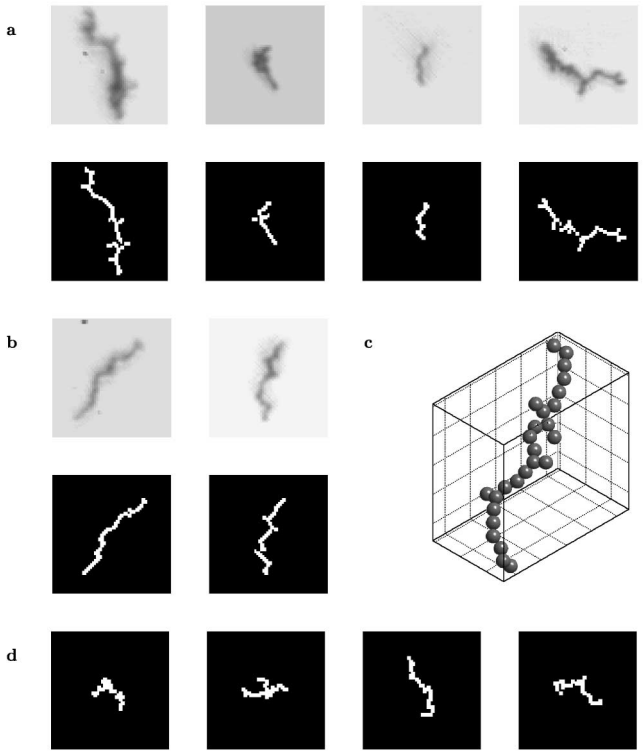

FIG. 1. Preplanetary dust analogs. (a) Raw images taken by the long-distance microscopes in the CODAG experiment (top row). Image analysis leads to the corresponding pictures in the bottom row from which the geometrical cross section, the radius of gyration, and the internal mass distribution were determined. Image sizes are $60 \times 60\ \mu$m^2. (b) Same as (a) but for two mutually perpendicular projections of the same aggregate, simultaneously observed by two long-distance microscopes. (c) Three-dimensional reconstruction of the aggregate in (b). The radius of each of the constituent spheres is 0.95 μm. (d) Simulated ballistic cluster-cluster aggregates, each consisting of 32 monodisperse spheres and grown with a restricted normalized impact parameter of $\psi > 0.65$. The images are to scale with the images in (a) and (b) and were reduced to the spatial resolution of the CODAG optical instrument. Detailed analysis of the internal mass distribution shows an excellent agreement between these simulated aggregates and those measured with CODAG.

For each of the detected particles, we also obtained positions of their respective centers of mass for five consecutive images with a time resolution of 5 ms. From these image sequences we derived for each particle, after the subtraction of the general cloudlet motion, one-dimensional displacement data Δx with time bases of $\Delta t = 5, 10, 15, 20$ ms. The diffusion coefficient D and the gas-grain response time τ_f are related by $D = (kT\tau_f)/m$, where k denotes the Boltzmann constant. Classical diffusion theory yields

$$\langle \Delta x^2 \rangle = 2D\Delta t\left(1 - \frac{\tau_f}{\Delta t} + \frac{\tau_f}{\Delta t}\exp(-\Delta t/\tau_f)\right) \quad (2)$$

[17]. For $\Delta t \gg \tau_f$, this reduces to the well-known diffusion equation $\langle \Delta x^2 \rangle = 2D\Delta t$ [18]. Using Eq. (2), we converted the measured displacement data for the different

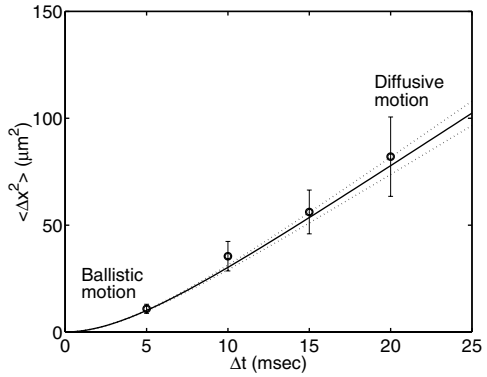

FIG. 2. Dust particle motion in the CODAG experiment. Mean square particle displacement $\langle \Delta x^2 \rangle$ as a function of sampling time Δt for the aggregates measured with the CODAG experiment (circles with error bars). For comparison with theoretical expectations, all displacements were corrected for their respective aggregate masses and were recomputed to monomer grains. The solid and the two dotted curves show the theoretical mean and range for pure diffusive motion with the expected value for the gas-grain response time $\tau_f = 4.3 \pm 0.3$ ms. For long sampling times $\Delta t \gg \tau_f$, the grain motion is diffusive, i.e., $\langle \Delta x^2 \rangle \propto \Delta t$; on shorter time scales, i.e., during an encounter between two grains, the particle motion is ballistic, i.e., $\langle \Delta x^2 \rangle \propto (\Delta t)^2$.

aggregate masses to mean square displacements for aggregates of unit mass m_0, which are plotted in Fig. 2 as a function of Δt (data points with error bars). From the measurement of the gas-grain friction time for monomers [19] and from the mass-to-surface ratio of simulated aggregate structures (see below), we computed an expected aggregate response time of $\tau_f = 4.3 \pm 0.3$ ms. The solid line in Fig. 2 shows the expected relation between the mean square displacement and sampling time [Eq. (2)]. From Fig. 2, we conclude that the measured displacements are consistent with pure Brownian diffusion.

For the mean net number of electrostatic charges on each monomer grain, we derived an upper limit of 2–3 elementary charges. The maximum electrostatic dipole moment on the dust aggregates is $p_{\max} = 4 \times 10^{-24}$ C m. Hence, the influence of electrostatic effects, such as attraction, repulsion, or alignment, is negligible for the local dynamics of the dust aggregates and the aggregation process itself, and the observed aggregate structures are a result only of the Brownian-motion-induced aggregation in rarefied gas and are to be considered as analogs to those expected to form in molecular clouds and during the formation of solar systems.

For the analysis of the internal structures of the aggregates, we determined their individual normalized internal mass distribution functions and compared these with theoretical representations of aggregation products. As a start, we performed numerical simulations of ballistic cluster-cluster aggregation (BCCA) [13]. The resulting BCCA aggregates have a fractal dimension of $D_f = 1.9$ [13] and were believed to represent the aggregates grown through thermal motion in rarefied gases. However, the internal mass distributions of the experimental aggregates do not match those of the BCCA aggregates. We interpret this deviation of the expected from the observed aggregate structures as being due to the influence of the hitherto neglected stochastic thermal rotation of the aggregates during a close approach. In the case of linear chains, the mean thermal circumference velocity is a factor of $\sqrt{3}$ larger than the mean thermal linear velocity of the chain aggregate. Qualitatively, the effect of thermal rotation is that the first contact of two aggregates being on a central collision course will take place between their outer constituents rather than their central parts. Therefore, the effective impact parameter of collisions with rotating aggregates will deviate from the theoretical value of central collisions of nonrotating aggregates. If we define the normalized impact parameter ψ such that central collisions have $\psi = 0$ and grazing collisions occur at $\psi = 1$, a slight restriction of the BCCA algorithm in the impact parameter space, $\psi > 0.65$, breaks the symmetry and produces aggregates whose internal mass distributions are in excellent agreement with those of the experimental aggregates. Examples of the simulated aggregates as they would appear in the CODAG microscope images are given in Fig. 1d.

One objective of the numerical simulations was to determine the mass-size relation [Eq. (1)] of the dust aggregates stemming from the ballistic thermal growth process. For the analog aggregates with $\psi > 0.65$, we determined $D_f = 1.3$. The ratio between mass and geometrical cross section is almost independent of the aggregate mass, and we get for the simulated aggregates $\tau_f \propto m^{0.06}$. Moreover, the numerical simulations allowed us to derive the masses of the observed aggregates from their geometrical cross sections by using the ratio between mass and geometrical cross section of the simulated aggregates. In Fig. 3a, the so-derived masses of the experimental aggregates are plotted versus the time of their occurrence after the dust injection (open circles).

With these aggregate masses and the known observational volumes, we determined the monomer number density in each of the two cloudlets. It turned out that both cloudlets had identical monomer number densities of $n_0 = 1 \times 10^{12}$ m^{-3}. The rectangular boxes in Fig. 3a represent the 1σ error of the mean aggregate mass in each of the cloudlets as well as the uncertainty of the mean time determinations.

For the derivation of the mass growth curve, the initial condition of the experiment needs to be known. Since there was no particle detection for $t < 50$ s, we performed control experiments in the laboratory, which showed that to a good approximation we can set $m(0) \approx (2 \pm 1)m_0$.

With the data in Fig. 3a, we cannot distinguish between an asymptotic growth of the form $m \propto t^2$ (solid line in Fig. 3a), as suggested by numerical simulations [12] and an exponential growth $m \propto \exp(t)$ (dashed line in Fig. 3a). The former is expected if the collision cross section between the aggregates is given by $\sigma_c \propto m$; the latter requires $\sigma_c \propto s^2 \propto m^{2/D_f}$ [13]. It is up to future models

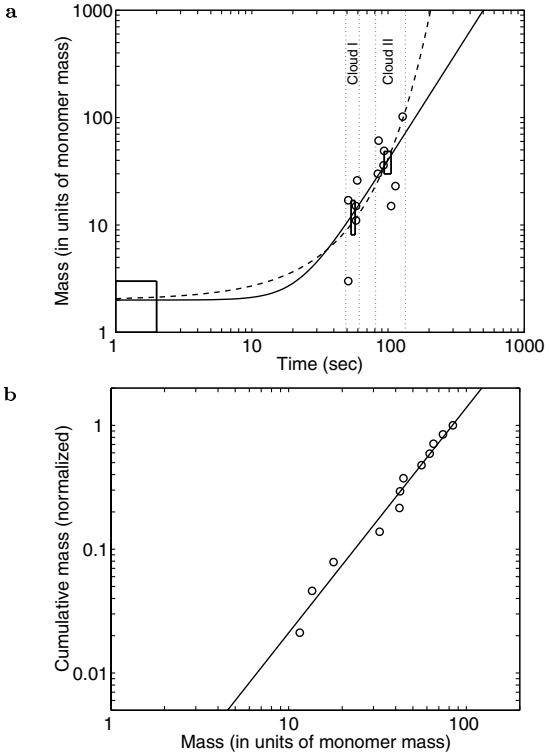

FIG. 3. Dust aggregate masses in the CODAG experiment. (a) Aggregate masses as a function of time after dust injection in the CODAG experiment. The open circles show the individual dust aggregates for which precise mass determinations were made. The rectangular boxes represent the 1σ error of the mean mass as well as the uncertainty of the mean time determinations for each of the two cloudlets (confined by the vertical dotted lines). The initial condition (rectangular box in the lower left corner of the diagram) was determined by calibration experiments in the laboratory. The dashed curve represents an exponential mass growth which is expected if the collision cross section is $\sigma_c \propto s^2 \propto m^{2/D_f}$, and the solid line has an asymptotic slope of 2 and represents a relation $\sigma_c \propto m$. Mind that both curves are meant only to guide the reader's eye. (b) Normalized cumulative mass spectrum of the aggregates in the CODAG experiment (open circles). To account for the different observation times, individual aggregate masses were extrapolated to $t = 100$ s with a power law of slope 2, matching the mean local slopes of the two curves in (a). The solid line is a least squares fit to the data points and has a slope of 1.8.

to derive the collision cross section for aggregates with arbitrary fractal dimensions and to compute the temporal evolution of the mean aggregate mass for Brownian motion and rotation. Figure 3b shows the corresponding mass spectrum of the observed dust aggregates. The data points fall along a well-defined power law with an exponent of $2 - \lambda = 1.8$. Thus, the mass spectrum reads

$$n(m)\mathrm{d}m \propto m^{-\lambda}\mathrm{d}m\,, \tag{3}$$

with $\lambda = 0.2$. The measured cumulative mass spectrum compares very well with the mass spectrum computed in [12], particularly for their highest monomer number density. A recent analysis of mass spectra derived by solving the coagulation equation also gives similar results [20]. Mass spectra with $\lambda < 2$ represent mass distributions that are dominated by the highest mass in the spectrum. In the mass distribution shown in Fig. 3b, 50% (90%) of the total mass are concentrated in aggregates whose masses are higher than 68% (28%) of the maximum mass. Hence, the mass distribution function in Brownian-motion-driven dust aggregation can be considered as quasimonodisperse.

In this paper, we showed that the initial stage of planetesimal formation in the solar nebula due to Brownian-motion-driven agglomeration proceeds rather rapidly and leads to previously unexpected open-structured, fractal dust aggregates with narrow mass distribution functions. Although electrostatic particle charging by solar irradiation is negligible in the young solar system due to the high opacity, other factors, such as magnetic fields, may affect early grain growth. Therefore, our experimental results are applicable for nonmagnetic dust grains only.

This work was supported by the German Space Agency DLR.

*To whom correspondence should be addressed.
Email address: blum@astro.uni-jena.de

[1] S. J. Weidenschilling and J. N. Cuzzi, in *Protostars and Planets III,* edited by E. Levy and J. I. Lunine (University of Arizona Press, Tucson, 1993), p. 1031.
[2] S. V. W. Beckwith, T. Henning, and Y. Nakagawa, in *Protostars and Planets IV,* edited by V. Mannings, A. P. Boss, and S. S. Russell (University of Arizona Press, Tucson, 2000), p. 533.
[3] W. Benz, Space Sci. Rev. (to be published).
[4] J. Blum, Space Sci. Rev. (to be published).
[5] S. J. Weidenschilling, Space Sci. Rev. (to be published).
[6] G. W. Wetherill and S. Inaba, Space Sci. Rev. (to be published).
[7] S. S. Barshay and J. S. Lewis, Annu. Rev. Astron. Astrophys. **14**, 81 (1976).
[8] J. F. Kerridge, Icarus **106**, 135 (1993).
[9] T. Poppe, J. Blum, and T. Henning, Astrophys. J. **533**, 454 (2000).
[10] G. Wurm and J. Blum, Icarus **132**, 125 (1998).
[11] J. Blum and G. Wurm, Icarus **143**, 138 (2000).
[12] S. Kempf, S. Pfalzner, and T. Henning, Icarus **141**, 388 (1999).
[13] P. Meakin, Rev. Geophys. **29**, 317 (1991).
[14] H. U. Keller *et al.,* Adv. Space Res. **13**, 73 (1993).
[15] J. Blum *et al.,* Meas. Sci. Technol. **10**, 836 (1999).
[16] G. Wurm and J. Blum, Astrophys. J. Lett. **529**, L57 (2000).
[17] S. W. Gardiner, *Handbook of Stochastic Methods for Physics, Chemistry, and the Natural Sciences* (Springer-Verlag, Berlin, 1985).
[18] A. Einstein, Ann. Phys. (Leipzig) **17**, 549 (1905).
[19] J. Blum, G. Wurm, S. Kempf, and T. Henning, Icarus **124**, 441 (1996).
[20] M. H. Lee, Icarus **143**, 74 (2000).